Mechanisms of stress generation and relaxation during pulsed laser deposition of epitaxial Fe–Pd magnetic shape memory alloy films on MgO

New Journal of Physics
The open-access journal for physics

Mechanisms of stress generation and relaxation during pulsed laser deposition of epitaxial Fe–Pd magnetic shape memory alloy films on MgO

Tobias Edler[1,3], Jörg Buschbeck[2], Christine Mickel[2], Sebastian Fähler[2] and S G Mayr[1]

[1] I. Physikalisches Institut, Georg-August-Universität Göttingen, Friedrich-Hund-Platz 1, 37077 Göttingen, Germany
[2] IFW Dresden, Institute for Metallic Materials, PO Box 270116, 01171 Dresden, Germany
E-mail: tobias.edler@physik.uni-goettingen.de

New Journal of Physics **10** (2008) 063007 (11pp)
Received 2 February 2008
Published 5 June 2008
Online at http://www.njp.org/
doi:10.1088/1367-2630/10/6/063007

Abstract. Mechanical stress generation during epitaxial growth of Fe–Pd thin films on MgO from pulsed laser deposition is a key parameter for the suitability in shape memory applications. By employing *in situ* substrate curvature measurements, we determine the stress states as a function of film thickness and composition. Depending on composition, different stress states are observed during initial film growth, which can be attributed to different misfits. Compressive stress generation by atomic peening is observed in the later stages of growth. Comparison with *ex situ* x-ray based strain measurements allows integral and local stress to be distinguished and yields heterogeneities of the stress state between coherent and incoherent regions. In combination with cross-sectional TEM measurements the relevant stress relaxation mechanism is identified to be stress-induced martensite formation with (111) twinning.

[3] Author to whom any correspondence should be addressed.

Contents

1. Introduction

Fe–Pd single crystals around the $Fe_{70}Pd_{30}$ composition exhibit the magnetic shape memory (MSM) effect, which allows the extension of a sample to be changed by up to several per cent by an external magnetic field [1]–[3]. For miniaturization in microactuators and on-chip integration, MSM thin films are desirable, which has motivated several groups to study polycrystalline Fe–Pd thin films [4]–[8]. However, strains exceeding 1% are only expected for single crystals and epitaxial films. Recently, it has been shown [9] that epitaxial Fe–Pd films can be grown at room temperature on MgO(100) single crystals by pulsed laser deposition (PLD), which is particularly advantageous for integration into microsystems. In these experiments, the fct phase formation range (suitable for the MSM effect) is observed in a significantly broader composition range than in the bulk, which has been related to stress-induced martensite formation. Additionally, it has been speculated that an unexpected (111) twinning observed in thicker films is also stress induced. The aim of this work is to examine in detail the stress within Fe–Pd films and to identify the underlying mechanisms.

2. Experimental details

Fe–Pd films were grown on MgO (100) substrates (dimensions 5 mm × 30 mm × 0.13 mm) at room temperature by deposition from elemental targets using PLD (KrF 25 ns 248 nm) under ultra high vacuum (UHV) conditions ($<10^{-8}$ mbar). The composition was adjusted by varying the number of laser pulses fired on each target. More details can be found in [9]. The compositions of the samples examined here were determined to be $Fe_{80}Pd_{20}$, $Fe_{70}Pd_{30}$ and $Fe_{60}Pd_{40}$, respectively, by energy dispersive x-ray analysis (EDX) measured using a $Fe_{70}Pd_{30}$ bulk standard. For comparison a pure Fe film was also prepared. From previous experiments it is known that films with Pd contents $\geqslant$29 at.% exhibit fct structure, whereas films with Pd contents $>$28 at.% (and elemental Fe) exhibit bcc structure at room temperature. It is furthermore known that bcc and bct films exhibit highly perfect epitaxial growth throughout the whole film thickness, whereas for fct films the epitaxial growth is disturbed by (111) twinning after a certain film thickness is exceeded. X-ray diffraction (XRD) measurements indicate that this critical thickness decreases when approaching the fct–bct transition [9].

The biaxial film growth stresses are determined with an instrumental resolution of $\approx$8 MPa nm by a substrate curvature measurement, using a two-laser-beam deflection dilatometer, as described before [10, 11]. Here, we ensured an unconstrained bending of the substrate by clamping it on a short side, while the free length was about 25 mm. The modified

Stoney equation [12]

$$\langle\sigma\rangle d = \frac{1}{6}\frac{E_s}{1-\nu_s}s^2\kappa \tag{1}$$

is employed to map curvatures, κ, to average film stresses, $\langle\sigma\rangle$, where d, s, E_s and ν_s denote the film thickness, substrate thickness, Young's modulus and Poisson's ratio of the substrate, respectively. The incremental stress $\frac{\partial(\langle\sigma\rangle d)}{\partial d}$ is usually the most meaningful quantity, as it corresponds to stress change in response to newly deposited material on top of the film. In the following, we use the convention that tensile stresses correspond to negative stress values.

Structural and microstructural characterizations were performed using XRD, transmission electron microscopy (TEM) and atomic force microscopy (AFM) investigations. Cross-sectional TEM samples were prepared using conventional ion beam thinning from sandwiched (face-to-face) film samples after diamond saw cutting and thin grinding to approximately 20 μm thickness; imaging was performed using a TECNAI T20 TEM with 200 kV and LaB_6 cathode. XRD in Θ–2Θ geometry was measured with Phillips X-Pert setup using Co K_α radiation.

Using the $\sin^2\Psi$-method [13], XRD was also applied for measuring the integral, biaxial in-plane film strain in a Phillips X-Pert 4-circle diffractometer. Recently, this method had been used to measure stress in post-annealed and epitaxial NiMnGa films [14, 15]. In the $\sin^2\Psi$-method, 2Θ of Bragg reflections is measured at different tilt angles Ψ. Whereas for polycrystalline materials one set of planes is used and measured for different tilt angles, this is not possible in our epitaxial films. Instead different sets of $\{hkl\}$ poles at distinct Ψ and Φ angles are measured. From 2Θ, the cubic lattice constant is calculated. For an angle of $\Psi = 0^\circ$, one obtains the lattice constant perpendicular to the surface of the film. By extrapolating the measured lattice constants to $\Psi = 90^\circ$, the in-plane lattice constant can be determined by fitting a linear behavior to the lattice constant plotted against $\sin^2\Psi$. For an angle of $\Psi = 45^\circ$, the unstrained lattice constant is expected for materials with a Poisson ratio of $\nu = 1/3$. From this lattice constant a_0 one can determine the in-plane strain ϵ, which is used to determine the in-plane stress σ using Young's modulus and Poisson's ratio of the film. Even if the elastic constants are not known accurately for a film, a positive slope of ϵ plotted against $\sin^2\Psi$ indicates a tensile in-plane stress, and a negative slope indicates a compressive stress, respectively.

3. Results

In substrate curvature-based stress measurements (figure 1) a clear compositional dependence is evident. Generally, films with the highest Fe content (Fe and $Fe_{80}Pd_{20}$) grow in the bcc phase with allover compressive stresses, while addition of more Pd ($Fe_{70}Pd_{30}$ and $Fe_{60}Pd_{40}$) results in fct structured films with early stage tensile and late stage compressive incremental stresses. In detail, almost constant incremental compressive stresses of (220 ± 10) MPa are observed over the whole film thickness regime in pure bcc Fe films. Bcc $Fe_{80}Pd_{20}$ films are characterized by generation of strong compressive stresses for $d < 40$ nm and reduced compressive stresses of (37 ± 7) MPa during later stages of film growth. $Fe_{70}Pd_{30}$ and $Fe_{60}Pd_{40}$ reveal tensile stresses of (-4.64 ± 0.03) and (-1.5 ± 0.05) GPa for thicknesses below 10 and 5 nm, respectively, whereas compressive incremental stresses of (240 ± 10) and (300 ± 10) MPa are observed for thicknesses exceeding 40 and 20 nm, respectively. In this context, we would like to note that interruption of the deposition process for several minutes did not result in any modification of the observed stress curves within an accuracy of 10 MPa, thus excluding artifacts, e.g. due to

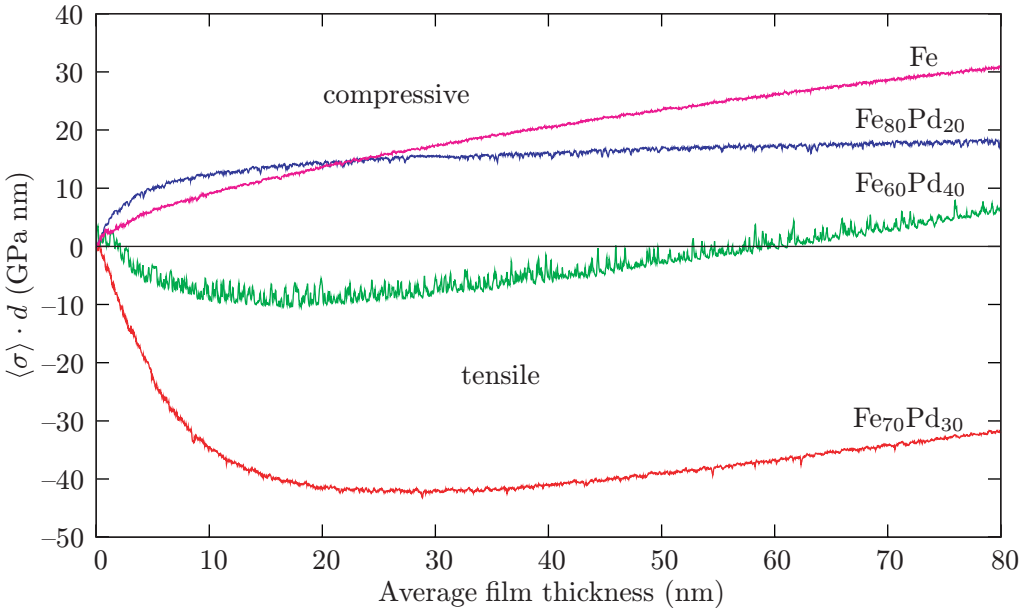

Figure 1. *In situ* substrate curvature during PLD of Fe–Pd films with different compositions. Positive and negative slopes correspond to compressive and tensile stress, respectively.

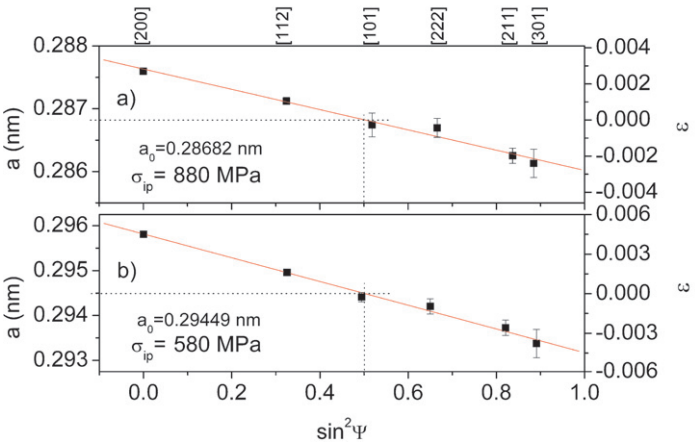

Figure 2. XRD measurement of the lattice constant and calculated relative strain for a pure Fe (a) and a $Fe_{80}Pd_{20}$ (b) film as a function of the substrate tilt Ψ. The stress is calculated from the strain using the extracted unstrained lattice constant a_0, literature values for Young's modulus E (see text) and Poisson's ratio $\nu = 1/3$. $\sin^2(\Psi) = 0$ and 1 correspond to the lattice constant perpendicular to the film surface, and the in-plane lattice constant, respectively.

substrate heating while linear drift of the instrument cancels out due to the employed two-laser-beam technique [10].

As an independent method, the $\sin^2\Psi$ method was applied for evaluating the stress state in the pure Fe film and $Fe_{80}Pd_{20}$ sample *ex situ*. Two ordinates were plotted in both graphs in figure 2—the absolute lattice constant measured (left axis) and the relative strain (right axis).

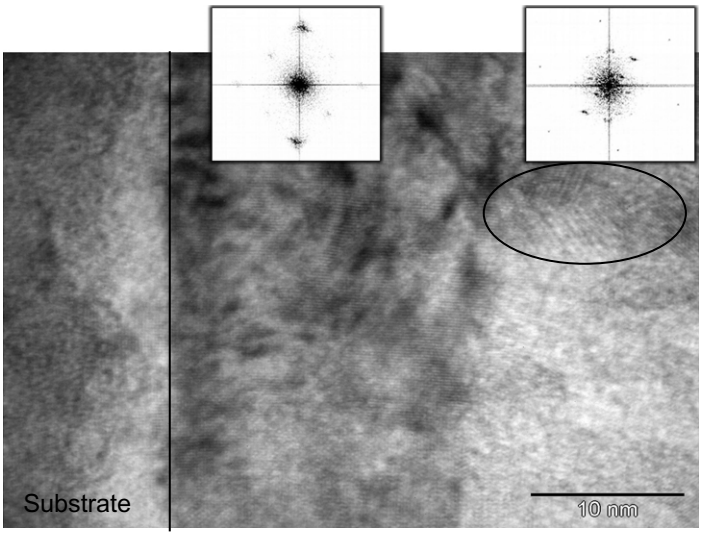

Figure 3. Cross-sectional bright field TEM micrograph of a $Fe_{70}Pd_{30}$ film. Three regions can be distinguished: the substrate on the left, a 20 nm thick, highly textured epitaxial Fe–Pd layer, and a region where epitaxy stresses are released by nucleation of twins (marked by a circle). The insets show typical Fourier transforms. Close to the substrate, the film is well-oriented, close to the free surface the orientation is distorted.

In agreement with the substrate bending experiments a negative slope is observed, proving compressive stress in the films. Higher relative strain is found for the $Fe_{80}Pd_{20}$ sample. By using Young's moduli of $E = 208$ GPa for bulk Fe [16] and $E = 86$ GPa for bulk $Fe_{80}Pd_{20}$ [17] and assuming Poisson's ratio of $\nu = 1/3$, the calculated stress in the Fe film is $\sigma_{ip} = 880$ and 580 MPa in $Fe_{80}Pd_{20}$ film, respectively. This differs significantly from the absolute value of stress measured using the substrate bending method, which will be discussed in section 4.

A cross-sectional TEM image of a $Fe_{70}Pd_{30}$ film (figure 3) shows two different regions with different contrasts. The transition between both the regions occurs at about 20 nm film thickness. The fast Fourier transformations (FFT) of both the regions allow to identify highly textured growth close to the substrate and a (111)-twinned microstructure at further distance. The first 20 nm of the film exhibits a wavy and spotty cross-sectional contrast. These features are typical for stressed TEM samples and are caused by the relaxation of film stress leading to surface modulation after preparation of the TEM lamella. This local measurement thus agrees well with the integral stress measurements indicating severe stress at the first nanometers of film growth. The image also shows a twin boundary, which starts right at the transition thickness.

To obtain information on the initial film growth morphology, AFM measurements were performed. Figure 4 shows the morphology of 5 nm thin films with compositions in the fct range. All samples show droplets, which are a typical side-effect of films grown by UHV–PLD: when the target is rapidly heated by the laser pulse, not only single atoms are ejected from the plasma plume, but as the target roughens during deposition also larger (at least partially molten) parts of the target are ablated [18]. These drops can reach the substrate and form droplets with a typical size of 50 nm up to several microns. Apart from the droplets, they reveal a different growth mechanism: while the film with the high Pd content shows granular growth with small

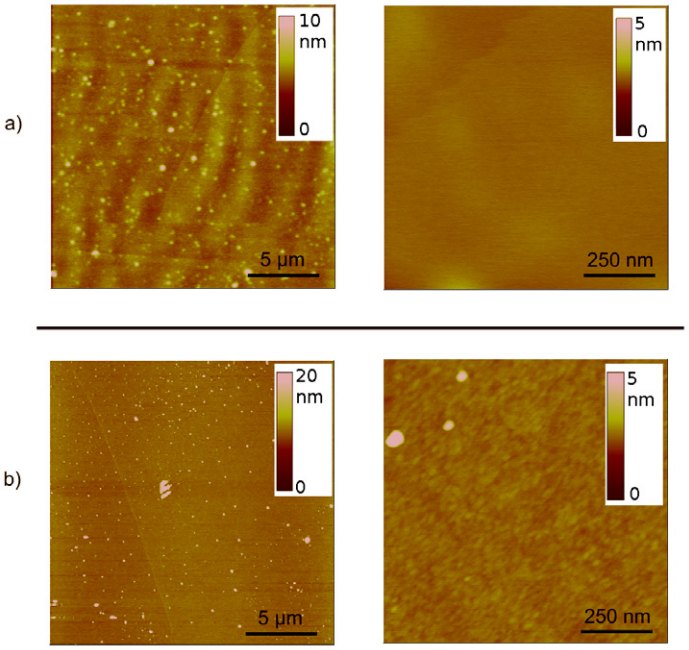

Figure 4. AFM topographs of 5 nm thick Fe–Pd films. (a) $Fe_{70}Pd_{30}$, showing a long-ranged rippled structure in the overview (left), but a very smooth structure with no signs of islands in the higher magnification (right) (RMS roughness: 0.493 nm for the picture on the left, 0.180 nm for the picture on the right); (b) $Fe_{63}Pd_{37}$, showing smooth growth in the overview (left) and indications of initial island-like granular film growth with islands of 30 nm in diameter in the larger magnification (right). (RMS roughness: 0.312 nm (left) and 1.01 nm (right).) Particularly in the overview scan droplets are visible (bright and irregular arranged spots), which are a typical side effect of UHV PLD and are caused during ablation of target material [18].

islands with a diameter of approx. 30 nm, the film with the lower Pd content reveals continuous growth with a significantly broader wavy structure with a size of several microns. At this film thickness of 5 nm, indications for initial discontinuous film growth are observed for the $Fe_{63}Pd_{37}$ (increased RMS roughness). However, the AFM topograph does not show separated islands at this film thickness. Since only topography and not crystallographic orientation is probed, AFM measurements do not allow a confirmation of differently oriented crystallographic variants, though such large variant spacings are predicted for very thin (100) epitaxial films [19].

4. Interpretation and discussion

When our films are thick enough, compressive stresses at different levels are observed for all examined compositions. This suggests considering the deposition method as one major origin of stresses. In fact, kinetic energy transfer by the incident particles during PLD is expected to influence stresses, as reported before for PLD [20]–[23], sputter deposition [24] or ion bombardment [25]: kinetic energies of the deposited ions during PLD reach values

Table 1. Lattice constants of the Fe–Pd films and the MgO substrate, taken from [9].

Material	Structure	Lattice constant a	Lattice constant c
Fe	bcc	0.2879 nm	
$Fe_{80}Pd_{20}$	bcc	0.2960 nm	
$Fe_{70}Pd_{30}$	fct	0.3832 nm	0.3657 nm
$Fe_{60}Pd_{40}$	fct	0.3826 nm	0.3699 nm
MgO	cubic	0.421 nm	

up to 100 eV [26] and thus result in implantation effects, viz. the creation of point defects—presumably with a surplus of interstitials. The positive formation volumes of interstitials result in an overall compressive stress contribution. Variation in film composition can influence stress generation by implantation in a threefold way: (i) interstitials of different atomic species will almost certainly reveal different formation volumes, (ii) the mobility of interstitials in alloys can be severely modified, thus resulting in a modified annihilation rate at sinks (such as vacancies or the open surface), increased interstitial mobility of Cu has been reported in literature e.g. for Cu doped bcc Fe [27] and (iii) different epitaxy strains can strongly affect interstitial migration enthalpies, and presumably even bias the direction of interstitial migration. When considering our stress measurements in the thick film limit (figure 1), significantly lower compressive stresses are observed in $Fe_{80}Pd_{20}$ in comparison to the other samples. The non-monotonous behavior of the stress in this film suggests the superposition of different stress relaxation mechanisms. This might be caused by the alloying of Fe with Pd as well as the higher kinetic energy of Pd atoms and ions, compared to Fe causing generation of increased number of point-defect in $Fe_{80}Pd_{20}$ compared to pure Fe.

As long as epitaxy strictly holds (which is the case in the thin film regimes) misfit of film and substrate is known as a prominent source of film stresses (see e.g. [28] and references therein). Epitaxial relationship and lattice constants of Fe–Pd films on MgO have been measured by 4-circle XRD in a previous work [9] and are summarized in table 1. As films exhibiting the fct structure grow cube-on-cube, whereas bcc films grow with a 45° rotation on the MgO(100) substrate, the corresponding misfit strains are calculated from $(a_{\mathrm{FePd}} - a_{\mathrm{MgO}})/a_{\mathrm{MgO}}$ and $(\sqrt{2}a_{\mathrm{FePd}} - a_{\mathrm{MgO}})/a_{\mathrm{MgO}}$ for fct and bcc, respectively.

Pure bcc Fe films grow epitaxially throughout the complete film thickness and have a predicted misfit of −3% which suggests tensile stress. However, contrary to this expectation an almost constant compressive stress exists within the complete film. This observation suggests that epitaxy related misfit stress contributions are compensated by PLD related compressive contributions, as discussed above. $Fe_{80}Pd_{20}$ films grow epitaxially throughout the complete thickness with a misfit of −0.6%, hence only minor tensile epitaxy stresses are expected. We therefore attribute the overall compressive stresses at least partially to energetic deposition, as discussed above. The rather high (≈0.8 GPa) compressive stresses for thicknesses <5 nm might be related to capillary driven effects.

The $\sin^2\Psi$-method also yields compressive stresses for both the bcc films, but the absolute values are significantly higher. A similar difference has been reported by other authors. In experiments on ion irradiation of tungsten films a deviation of a factor of about 2 was

observed [29], whereas experiments on ion irradiation of stainless steel sheets yielded a factor of about 9 [30, 31]. This suggests that x-ray strain measurements only probe subvolumes of the whole film. In fact, while substrate curvature measures the average stress of all grains including internal and external interfaces within the film, XRD is an indirect probe, only measuring the strain within coherently scattering regions. With this, XRD ignores incoherently scattering regions like grain boundaries etc, where stress relaxation preferentially occurs. Though grown epitaxially, the coherence length of the bcc films is below 20 nm [9], suggesting that a significant stress relaxation has occurred in these incoherent regions. The deviation between the results of the two methods is smaller for thick films having a larger grain size [32].

For substrate curvature measurements the Stoney equation only requires the well-known Young's modulus of the substrate. The $\sin^2\Psi$-method, however, measures the deviation of lattice constants in the film. The calculation of the associated stress thus requires knowledge of the elastic constants of the film. For monolayer thin films, the bulk value is not valid, but the films examined here are relatively thick (above 80 nm), so that the bulk values can be considered as a reasonable approximation. Measurements using the $\sin^2\Psi$-method are only presented for completely epitaxially grown cubic films, where bulk data of a similar composition is available. For non-cubic martensite this method fails since one cannot distinguish between an elastic tetragonal distortion or structural inherent tetragonal distortion-like in a stress-induced martensite.

However, the application of the $\sin^2\Psi$-method is limited to films with a cubic structure (Fe and $Fe_{80}Pd_{20}$). For films with a tetragonal fct structure ($Fe_{70}Pd_{30}$ and $Fe_{60}Pd_{40}$), one cannot derive the film stress from the tetragonal distortion.

Stress-induced martensite formation is a typical phenomenon in martensitically transforming alloys. In the martensite, stress relaxation occurs not via the tetragonal distortion (c/a ratio), but by changing the population of the different variant orientations. This is easily possible until one variant orientation is exhausted and allows for the compensation of high strains of up to 6% in Fe–Pd.

Both films exhibit a quite large negative misfit of -9% (fct a-axis) and -12% (fct c-axis) with respect to the MgO(100) substrate. Due to this high misfit to the substrate, a significantly higher tensile stress is expected and indeed observed in thin fct films. According to the model of stress induced martensite, this favors the formation of martensite in the films. In Fe–Pd bulk martensite, a broad range of c/a ratios are observed in the fct phase at different temperatures and compositions. The c/a ratios observed here are close to the maximum value of 6% observed in bulk at low temperatures [2], indicating that a further tetragonal distortion is not energetically favored in this system. Previous XRD measurements [9] also show that not all possible martensitic variant orientations are observed, but only variants with one long a- and the short c-axis in-plane exist in these films. Variants with both longer a-axis in-plane have not been observed, which is in agreement with the measured tensile stress. In films with higher Pd content, a tensile stress is also observed, but the absolute value is significantly lower compared to that of the $Fe_{70}Pd_{30}$ film. In accordance with the AFM topology, showing granular growth this indicates that a part of the stress has been reduced at the cost of the formation of increased surface (energy) in this film.

From the integral XRD investigation published previously [9] it was suggested that fct films should grow epitaxially up to a thickness of 20 nm, whereas films with higher thickness also exhibit misorientations possibly caused by (111) twinning, as they have also been observed in chemically ordered $Fe_{50}Pd_{50}$ films [33]. This is confirmed by the presented TEM micrographs.

The transition thickness between highly textured and (111) twinned, misoriented film growth observed in XRD and TEM coincides with the change in slope of the curvature measurement in the Pd rich fct films also occurring around 20 nm. This also supports the picture that the (111)-twinning effectively reduces the stress in the film. In these integral measurements the transition, however, is not as sharp as observed in TEM, as the large substrate used results in a thickness gradient of about $\pm 10\%$.

Though in thin films (100)-oriented epitaxial growth is obviously energetically favorable as film and substrate have an identical symmetry, large tensile stresses are induced, which cannot be completely compensated by the martensite formation. In the course of further film growth the elastic energy thus further increases, until defect nucleation becomes favorable, thus relieving misfit for the following layers. Typically, this occurs by the introduction of misfit dislocations. Here, we identify (111) twin-boundary formation as the predominant strain relaxation mechanism. During further film growth, compressive stress due to energetic deposition becomes apparent.

5. Conclusion

In situ stress measurements give a significantly more detailed understanding of Fe–Pd film growth compared to integral *ex situ* methods. In addition to the conventional effects, shape memory alloys exhibit the freedom of a stress induced martensitic phase transformation. This allows epitaxial growth of martensite on substrates with large misfits. For thicker films (111) twinning as an additional stress relaxation mechanism is observed, and the epitaxial relationship to the substrate is lost. Similar twinning has been reported also for other material systems like silicide films [34, 35] and gold films [36] suggesting that the examined mechanism is important for a broad range of materials. Thus, large tensile stress in thin epitaxial films and for thicker films compressive stress originating from energetic deposition can be reduced. These experiments identified the different origins of film stress inhibiting the growth of thick, epitaxial films. Thus, they are a key step towards thick films suitable for MSM microactuators and sensors.

Acknowledgments

We thank C Mahn for the technical support. Funding through the DFG Priority Program SPP 1239 is gratefully acknowledged.

References

[1] James R D and Wuttig M 1998 Magnetostriction of martensite *Phil. Mag.* A **77** 1273
[2] Kakeshita T and Fukuda T 2001 Giant magnetostriction in Fe_3Pt and FePd ferromagnetic shape-memory alloys *Mater. Sci. Forum* **394** 531
[3] Cui J, Shield T W and James R D 2004 Phase transformation and magnetic anisotropy of an iron–palladium ferromagnetic shape-memory alloy *Acta Metall.* **52** 35–47
[4] Wang Z 2000 Structural characteristics and magnetic properties of Fe–Pd thin films *Int. J. Appl. Electromagn. Mech.* **12** 61–6
[5] Sugimura Y, Cohen-Karni T, McCluskey P and Vlassak J 2003 Fabrication and characterization of Fe–Pd ferromagnetic shape-memory thin films *Mater. Res. Soc. Symp. Proc.* **785** D7.4.1

[6] Vokoun D, Shih J C, Chin T S and Hu C T 2004 Magnetic properties of Fe–30 at% Pd films *J. Magn. Magn. Mater.* **281** 105–9
[7] Wang F, Doi S, Hosoiri K, Yoshida H, Kuzushima T, Sasadaira M and Watanabe T 2006 Nanostructured Fe–Pd thin films for thermoelastic shape memory alloys electrochemical preparation and characterization *Electrochim. Acta* **51** 4250–4
[8] Kock I, Edler T and Mayr S G 2008 Growth behavior and intrinsic properties of vapor-deposited iron palladium thin films *J. Appl. Phys.* **103** 046108
[9] Buschbeck J, Lindemann I, Schultz L and Fähler S 2007 Growth, structure, and texture of epitaxial $Fe_{100-x}Pd_x$ films deposited on MgO(100) at room temperature: an x-ray diffraction study *Phys. Rev.* B **76** 205421
[10] Bicker M, von Hülsen U, Laudahn U, Pundt A and Geyer U 1998 Optical deflection setup for stress measurements in thin films *Rev. Sci. Instrum.* **69** 460
[11] Mayr S G and Samwer K 2001 Model for intrinsic stress formation in amorphous thin films *Phys. Rev. Lett.* **87** 36105
[12] Stoney G G 1909 The tension of metallic films deposited by electrolysis. *Proc. R. Soc. Lond.* A **82** 172–5
[13] Birkholz M 2006 *Thin Film Analysis by X-Ray Scattering* (New York: Wiley)
[14] Doyle S, Chernenko V A, Besseghini S, Gambardella A, Kohl M, Müllner P and Ohtsuka M 2008 Residual stress in NiMnGa thin films deposited on different substrates *Eur. Phys. J. Spec. Top.* **158** 99–105
[15] Thomas M, Heczko O, Buschbeck J, Schultz L and Fähler S 2008 Stress induced martensite in epitaxial Ni–Mn–Ga films deposited on MgO(001) *Appl. Phys. Lett.* **92** 192515
[16] Cardarelli F 2000 *Materials Handbook* (Berlin: Springer)
[17] Nakayama T, Kikuchi M and Fukamichi K 1980 Young's modulus and the Delta E effect of Fe–Pd invar alloys *J. Phys. F: Met. Phys.* **10** 715–9
[18] Fähler S, Störmer M and Krebs H U 1997 Origin and avoidance of droplets during laser ablation of metals *Appl. Surf. Sci.* **109** 433–6
[19] Kiselev N S, Dragunov I E, Onisan A T, Rößler U K and Bogdanov A N 2008 Theory of stripe domains in magnetic shape memory alloys *Eur. Phys. J. Spec. Top.* **158** 119–24
[20] Störmer M, Sturm K, Fähler S, Weisheit M, Winkler J, Kahl S, Kesten Ph, Pundt A, Seibt M, Senz S and Krebs H-U 1999 Study of laser-deposited metallic thin films by a combination of high-resolution *ex situ* and time-resolved *in situ* experiments *Appl. Phys.* A **69** 455–7
[21] Krebs H U, Bremert O, Luo Y, Fähler S and Störmer M 1996 Structure of laser-deposited metallic alloys and multilayers *Thin Solid Films* **275** 18–21
[22] Sakai H, Keitoku S and Ezumi H 1997 Contribution of high-velocity particles to stress of thin film produced by laser ablation *Japan. J. Appl. Phys.* **36** L409–11
[23] Mayr S G, Moske M, Samwer K, Taylor M E and Atwater H A 1999 The role of partical energy and pulsed pulsed partical flux in physical vapor deposition and pulsed–laser deposition *Appl. Phys. Lett.* **75** 4091
[24] Thornton J A and Hoffmann D W 1989 Stress-related effects in thin films *Thin Solid Films* **171** 5–31
[25] Mayr S G and Averback R S 2003 Effect of ion bombardment on stress in thin metal films *Phys. Rev.* B **68** 214105
[26] Fähler S and Krebs H U 1996 Calculations and experiments of material removal and kinetic energy during pulsed laser ablation of metals *Appl. Surf. Sci.* **76** 61–5
[27] Marian J, Wirth B D, Perlado J M, Odette G R and Diaz de la Rubia T 2001 Dynamics of self-interstitial migration in Fe–Cu alloys *Phys. Rev.* B **64** 094303
[28] Mayr S G 2001 Mechanical stresses in thin films *Encyclopedia of Materials: Science and Technology* ed K H J Buschow, R W Cahn, M C Flemings, B Ilschner, E J Kramer and S Mahajan (Amsterdam: Elsevier) pp 9279–83
[29] Durand N, Badawi K F and Goudeau P 1996 Residual stresses and microstructure in tungsten thin films analyzed by x-ray diffraction-evolution under ion irradiation *J. Appl. Phys.* **80** 5021
[30] Wang Q, Ogiso H, Nakano S, Akedo J and Ishikawa H 2003 Martensitic transformation and the stress induced by 3 MeV ion implantation in an austenite stainless steel sheet *Nucl. Instrum. Methods* B **206** 118–22

[31] Wang Q, Ishikawa H, Nakano S, Ogiso H and Akedo J 2004 Curvature-based residual stress measurement for ion-implanted stainless-steel sheet *Vacuum* **75** 225–9

[32] Ravet M F, Badawi K F, Durand N, Lafontaine H, Barnole V and Haghiri-Gosnet A M 1993 *Mater. Res. Soc. Symp. Proc.* **306** 259

[33] Halley D, Samson Y, Marty A, Bayle-Guillemaud P, Beigné C, Gilles B and Mazille J E 2002 Anomaly of strain relaxation in thin ordered FePd layers *Phys. Rev.* B **65** 205408

[34] Eaglesham D J, Tung R T, Sullivan J P and Schrey F 1993 Interfacial defects in silicides on Si (100): coreless defects, $1/12\langle 111\rangle$ dislocations, and twinning mechanisms *J. Appl. Phys.* **73** 4064

[35] Onda N, Sirringhaus H, Muller E and von Kanel H 1993 Structural and electronic properties of pseudomorphic $FeSi_{(1+x)}$ films on Si (111) *J. Cryst. Growth* **127** 634–7

[36] Dehm G, Oh S H, Gruber P, Legros M and Fischer F D 2007 Strain compensation by twinning in Au thin films: experiment and model *Acta Mater.* **55** 6659–65